

An improved first-principles density functional theory for the solution of band gap problems in IV and III-V semiconductors

Sujoy Datta,^{1,2} Prashant Singh,^{3,*} Chhanda B. Chaudhuri,² Debnarayan Jana,¹ Manoj K. Harbola,⁴ Duane D. Johnson,^{3,5} and Abhijit Mookerjee^{2,6}

¹*Department of Physics, University of Calcutta, Kolkata 700009, India*

²*Department of Physics, Lady Brabourne College, Kolkata 700017, India*

³*Division of Materials Science & Engineering, Ames Laboratory, Ames, Iowa 50011, USA*

⁴*Department of Physics, Indian Institute of Technology, Kanpur, 208016, India*

⁵*Department of Materials Science & Engineering, Iowa State University, Ames, Iowa 50011, USA*

⁶*S. N. Bose National Centre for Basic Sciences, Salt Lake City, Kolkata 700098, India*

(Dated: June 11, 2022)

We report results from a fast, efficient and first-principles full potential N^{th} order muffin tin orbital (FP-NMTO) method based approach for self-consistent calculations of electronic and structural properties of group IV and III-V semiconductors. We exemplify our implementation of van Leeuwen-Baerends (vLB) correction to local density approximation (LDA) exchange in FP-NMTO through Ge and GaAs. The distinctive feature of our computations stem from the use of non-relativistic FP-NMTO with vLB corrected LDA exchange correlation potential. Our results are in agreement with experiments, in particular, indirect nature of band-gap ($E_{\Gamma-L}$) in Ge and lattice constant, which most semilocal exchange-correlation functionals get wrong. Predicted (band-gap, equilibrium lattice constant, bulk modulus) for Ge (0.86 eV, 5.57Å, 75 GPa) and GaAs (1.42 eV, 5.656Å, 79 GPa) are in good agreement with experiments.

I. INTRODUCTION

Semiconducting materials have always been of great interest because of their central role in modern electronics.^{1–19} As we enter the era of designing optimal materials, it has become essential to quickly and accurately estimate the band-gaps of semiconductor materials. Similarly, experimentalists would benefit from an efficient computational tool for predicting band-gaps prior to synthesis. We consider the problem of predicting physical band-gaps to be solved by a computational method that delivers an accurate result for compounds spanning the whole periodic table and is simultaneously practical to compute. Standard exchange correlation (XC) functionals, such as the Perdew–Burke–Ernzerhof (PBE),^{20,21} have been the backbone of DFT based calculations for decades. Unfortunately, the unphysical self-Coulomb repulsion²² leads to a systematic underestimation of the band-gaps.^{23–25} On the other hand, including hybrid functionals such as Hartree-Fock exchange and Heyd-Scuseria-Ernzerhof functional²⁶ substantially reduces the Coulomb self-repulsion error.²⁷ However, the use of hybrid-functionals enhances the computational time considerably.²⁸

Improving XC-functionals within DFT formalism remains one of the active research areas.^{29–36} Better and a more accurate semi-local XC-functional has been constructed by satisfying a larger number of exact physical behaviors,^{32,37} by introducing increasingly more complicated dependence on the density.^{32,35} On the other hand, the semi-empirical formulas derived as corrections to the local density approximation (LDA) are fast, mathematically easy to handle and produce good results.^{38–46} These functionals incorporate the gradient of the den-

sity in such a way that the potential is asymptotically well behaved.^{42–44,46} The van Leeuwen-Baerends (vLB) corrected⁴¹ LDA has predicted band gaps in a range of bulk and nano-materials.^{42–47} These results were in good agreement with known theoretical and experimental values.

Despite this success, the vLB corrected LDA, as implemented in the tight-binding linearized muffin-tin orbital (TB-LMTO) basis underestimated the band-gaps of group IV and III-V semiconductors, in particular, those of Ge and GaAs. Since the LDA+vLB worked pretty well in most cases, instead of proposing some new XC-potential, we have tried to improve upon the basis set for the construction of the Hamiltonian.

Basis sets play a central role in improving electronic and structural behavior and material properties.^{48,49} Research has not only been limited to developing sophisticated functionals, but research has focused on the construction of basis sets which are complete and compact. The full potential N^{th} order muffin-tin orbitals (FP-NMTO) do not incorporate any atomic sphere like approximation (ASA) as in the LMTO.⁵⁰ So, a single compact basis set can be used to describe the entire system including the interstitial region. It is accurate whether the system is close-packed or not. In the TB-LMTO, energy dependence of the basis set is avoided by its Taylor expansion upto the first energy derivative.^{51,52} In the NMTO, on the other hand, a sophisticated interpolation scheme involving higher order derivatives is used,^{53–56} FP-NMTO provides a smaller and energy independent basis set comparable to most localized Wannier functions, which is a prerequisite for increased computational speed and efficiency. Moreover this present version of NMTO is totally self-consistent.

II. THEORETICAL DETAIL

A. vLB correction in LDA

The Kohn-Sham (KS) equation transforms the interacting many-electron system to a system of non-interacting electrons moving in an effective potential due

$$\begin{aligned} \mathbf{V}_{\text{eff}}(\vec{r}) &= \mathbf{V}_{\mathbf{H}}(\rho(\vec{r})) + \mathbf{V}_{\text{xc}}[\rho(\vec{r})] + \mathbf{V}_{\text{ie}}[\rho(\vec{r})] + \mathbf{V}_{\text{ext}} \\ &= \int d\vec{r}' \frac{\rho(\vec{r}')}{|\vec{r} - \vec{r}'|} + V_{\text{xc}}[\rho(\vec{r})] + \sum_{\vec{R}_n} \frac{Z^2 Q}{|\vec{r}' - \vec{R}_n|} + \sum_{\vec{R}_n \neq \vec{R}_m} \frac{Z^2 Q^2}{|\vec{R}_n - \vec{R}_m|} \end{aligned} \quad (1)$$

the Coulombic potentials have to be self-consistently obtained. The first term is the Hartree potential, second term is the exchange-correlation potential V_{xc} , the third arises from the ion-cores and finally the ion-ion re-

to all other electrons and ions. Using the Hohenberg-Kohn theorem, the Schrödinger's equation for many body system reduces to the so-called Kohn-Sham equation :

$$\mathbf{T}_{\text{eff}}[\rho(\vec{r})] + \mathbf{V}_{\text{eff}} \Psi(\vec{r}) = \mathbf{E} \Psi(\vec{r}) \quad (1)$$

where the effective potential is

pulsive potential V_{ext} .

The contribution to the total energy-functional of these effective potentials is given by :

$$\begin{aligned} \mathbf{E}[\{\Psi_\lambda\}, \{\vec{R}_n\}] &= - \sum_{\lambda \in \text{occ}} \int d\vec{r} \Psi_\lambda^*(\vec{r}) \nabla^2 \Psi_\lambda(\vec{r}) + \int d\vec{r} \rho(\vec{r}) V_{\text{ext}}(\vec{r}) + \dots \\ &\dots \iint d\vec{r} d\vec{r}' \frac{\rho(\vec{r})\rho(\vec{r}')}{|\vec{r} - \vec{r}'|} + E_{\text{xc}}[\rho(\vec{r})] + \sum_{\vec{R}, \vec{R}'} \frac{Z^2 Q^2}{|\vec{R} - \vec{R}'|} \end{aligned} \quad (3)$$

The local density approximation (LDA), first introduced by Slater, simplifies the non-local exchange energy in terms of the local $\rho^{1/3}$ potential.⁶³ The XC-energy density depends only on the local electron density $\rho(\vec{r})$ for each volume element $d\vec{r}$ around \vec{r} , i.e.

$$E_{\text{xc}}^{\text{LDA}} \simeq \int \rho(\vec{r}) \varepsilon_{\text{xc}}[\rho(\vec{r})] d\vec{r}$$

The local XC-energy density $\varepsilon_{\text{xc}}[\rho(\vec{r})]$ of a homogeneous electron gas has been calculated by many approaches: (a) many-body perturbation theory,⁶⁴ (b) Quantum Monte-Carlo.⁶⁵ Amongst these, LDA-XC potential by the Barth-Hedin is the most used,⁶¹ with the Ceperley-Alder parametrization.⁶⁵ These various forms have been described in the literature.^{66,67}

The LDA potential for finite systems decays exponentially similar to density. However, the potential should decay as $\sim (-1/r)$, i.e., Coulomb like.⁶⁸ Becke proposed a nonlocal correction to the energy-functional and then took the functional derivative to find the exchange potential.³⁸ This gave the correct form of exchange-energy density in the asymptotic region but failed to re-

produce the exact behavior for the potential. Perdew and Wang developed generalized gradient approximation (GGA) where a energy gradient term is added.^{21,69} Later van Leeuwen and Baerends provides a similar type of correction to the LDA exchange, which improved the eigenvalues for the highest occupied orbitals of atoms significantly.^{41,70-72} The corrected LDA+vLB potential can be written as:

$$v_{\text{xc}}(\vec{r}) = [v_x^{\text{LDA}}(\vec{r}) + v_x^{\text{LB}}(\vec{r})] + v_c^{\text{LDA}}(\vec{r}) \quad (4)$$

where,

$$v_x^{\text{LB}}(\vec{r}) = -\beta \rho^{1/3}(\vec{r}) \frac{x^2}{1 + 3\beta x \sinh^{-1}(x)} \quad (5)$$

with $x = |\vec{\nabla} \rho(\vec{r})| / \rho^{4/3}(\vec{r})$ and $\beta = 0.05$.

B. The classical Muffin-tin potential and partial wave solutions: LMTO vs NMTO

In the TB-LMTO muffin-tin spheres (atomic sphere approximation (ASA)) are used to describe both the

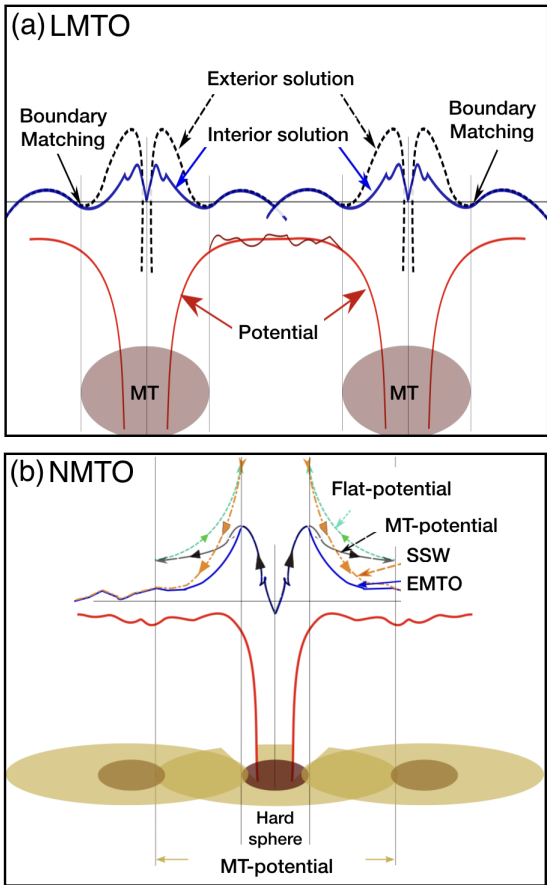


FIG. 1. (Color online) Schematic of atomic-spheres and corresponding potential within (a) tight binding linearized muffin-tin orbital method, and (b) Full potential N^{th} order muffin-tin orbital method based approaches.

variation of electronic charge as well as the potential. These spheres need to be space filling with optimal overlap ($\leq 15\%$). Overlap is essential for atomic bonding whereas too large an overlap of charge may lead to its over-counting. The potential for a given atom is reasonably long ranged but the atomic charge density is more localized around the same atom. Taking these ideas into account, in NMTO, there are two different classes of concentric spheres: potential spheres (MT spheres) of radius s and charge spheres (screening spheres or hard spheres) of radius a ($a < s$), see Fig.1(b). However, the overlap of potential spheres in NMTO can be as large as 50% so full potential approach is a pre-requisite both in AS and interstitials, shown in Fig.1(b).

The solutions of radial KS equations [Eq.1] for atomic-potential φ^{as} is continued from the core of atom towards the muffin-tin surfaces at $r=s$. This is matched with the solution for a flat part of potential (as in LMTO, this flat potential is taken as zero potential) φ^{int} , which is denoted by φ^0 . The φ^0 is valid up to the boundary of hard sphere surface ($r=a$). We do normalization at the boundary of hard sphere surface (a) such that $\varphi^0|_a = 1$. The normalized wave-functions are written with super-

script “a”:

$$\begin{aligned}\varphi_{R,l}^a(\epsilon, r) &\equiv \frac{\varphi_{R,l}(\epsilon, r)}{\varphi_{R,l}^0(\epsilon, a_R)} \\ \varphi_{R,l}^{0a}(\epsilon, r) &\equiv \frac{\varphi_{R,l}^0(\epsilon, r)}{\varphi_{R,l}^0(\epsilon, a_R)}\end{aligned}\quad (6)$$

The $\varphi_{Rl}^{0a}(\epsilon, r)$ is matched with screened spherical waves (SSW: ψ^a) continuously but with a kink at a and truncated in the region $a_R \leq r \leq s_R$. $\varphi_{Rl}(\epsilon, r)$ is truncated outside $0 \leq r \leq s_R$. The SSWs grow outwards, which are sorted in two groups depending on the values of (R,l,m) : active channels (subscript $A \equiv RL$) and passive channels (subscript $I \equiv RL$). The matching described above is for the active channels which are truncated inside hard spheres with kinks. The passive channels are substituted smoothly by φ^{as} inside hard spheres. Finally, a basis set with elements termed as Kinked Partial Waves (KPW), which are defined in all space, is formed as:

$$\begin{aligned}\phi_{Rlm}^a(\epsilon, r_R) &= [\varphi_{R,l}^a(\epsilon, r)_R - \varphi_{R,l}^{0a}(\epsilon, r_R)]Y_{l,m}(\hat{r}_R) \\ &\quad + \psi_{Rlm}^a(\epsilon, \vec{r}_R)\end{aligned}\quad (7)$$

Only the linear combination of KPWs $\sum_{RL \in A} \phi_{Rlm}^a(\epsilon_i, r_R) c_{Rlm,i}^a$ can be one of the solutions of KS equation but not the individual KPWs. A kink cancellation condition can be achieved such that the kink in any hard sphere can be cancelled by the sum of the kinks from the tails of KPWs from neighboring sites. The idea is similar as the tail cancellation of LMTO.

This basis set spanned by the KPWs is explicitly energy dependent. Energy dependent basis set slows down the calculation which was the problem in exact MTO (EMTO) formalism. In LMTO, energy dependence is removed by a self-consistent choice of energy ϵ_ν about which a Taylor series expansion of basis functions are performed. The series is truncated after first order term leading to an error $\propto (\epsilon - \epsilon_\nu)^2$ in the solution of KS equation. The energy independent set of basis functions, the so called NMTO are the superposition of KPWs at a mesh of energies (calculated self-consistently) using Newton's interpolation method such that:

$$\begin{aligned}|\chi^{0\dots N}\rangle &= \sum_{n=0}^N |\phi(\epsilon_n)\rangle L_n^{0\dots N} \\ &= |\phi[0]\rangle + |\phi[01]\rangle (E^{(0\dots N)} - \epsilon_0) + \dots + \\ &\quad |\phi[0\dots N]\rangle (E^{(N-1,N)} - \epsilon_{N-1})(E^{(0\dots N)} - \epsilon_0)\end{aligned}\quad (8)$$

Where, $\phi[0] \equiv \phi(\epsilon_0)$; $\phi[01] \equiv \frac{\phi(\epsilon_0) - \phi(\epsilon_1)}{\epsilon_0 - \epsilon_1}$ are the terms in divided difference table. The error in the solution of KS equation becomes :

$$\psi(\vec{r}) - \psi(\epsilon, \vec{r}) \propto (\epsilon - \epsilon_0)(\epsilon - \epsilon_1)\dots(\epsilon - \epsilon_n)\quad (9)$$

The formation of the SSWs are described in the Appendix.

C. Advantage of FP-NMTO over TB-LMTO

The improved basis set of FP-NMTO method is accurate, minimal and flexible. Accurate because the FP-NMTO basis solves the KS equation exactly for overlapping muffin-tin potentials. Orthonormalized FP-NMTOs are localized atom-centered Wannier functions, generated in real space with Green-function techniques, without projection from band states.⁷³ However, TB-LMTO lacks in all above. Increased computational time is the only downside of the FP-NMTO compared to TB-LMTO.

III. COMPUTATIONAL DETAIL

We apply self-consistent FP-NMTO+vLB approach to calculate electronic properties of group IV and III-V semiconductors, in particular, Ge and GaAs. For LDA, we use the Ceperley and Alder exchange-correlation functional as parameterized by Vosko-Wilk-Nusair.⁷⁴ The GGA calculations were carried out using the Perdew, Burke, and Ernzerhof (PBE) exchange correlation contribution.²⁰ The distinctive feature of our calculations is the use of FP-NMTO with improved basis set with respect to TB-LMTO method. The vLB correction is implemented both in TB-LMTO as well as in FP-NMTO. We use third order in energy derivatives of wave functions ($N = 3$) within NMTO to interpolate and make the basis energy independent. We use $8 \times 8 \times 8$ (with 29 irreducible points) k-point mesh for Brillouin zone sampling. TB-LMTO uses atomic-sphere approximation (ASA). The self consistent potential converged to a difference of 10^{-6} after several tens of iterations. In calculating the lattice constant, we utilized a least square fit of our data to the Murnaghan's equation of state.⁷⁵ The calculated lattice constant is less than 0.5% overestimated with respect to experiments.^{76,77} The equilibrium lattice constant is used to evaluate the bulk modulus.

IV. RESULTS.

In Fig.2, we plot the band structure and total density of states (DOS) for Ge. Ge, in ground state, crystallizes in the diamond $Fd\bar{3}m$ -structure.⁷⁸ Two equivalent Ge's are placed at $(0, 0, 0)$ and $(1/4, 1/4, 1/4)$ in a cubic cell with Empty spheres (ESs) at $(-1/4, -1/4, -1/4)$ and $(1/2, 1/2, 1/2)$. Both TB-LMTO and FP-NMTO use average Wigner-Seitz radius 1.387\AA for Ge. For FP-NMTO, the hard sphere radius is 0.971\AA . The FP-NMTO+LDA gives a direct band-gap of 0.19 eV at Γ , which shows small improvement over LMTO+LDA of 0.10 eV. Treating the interstitial region in same way, use of improved basis set makes FP-NMTO better. However, if we switch to FP-NMTO+PBE, the band-gap is improved to 0.33 eV, but the nature of band-gap remain direct and more than 50% underestimated with respect to

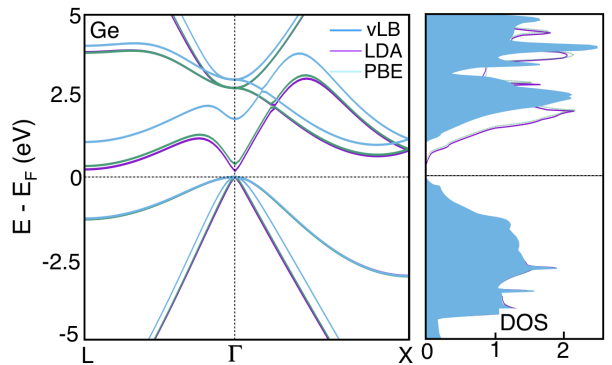


FIG. 2. (Color online) The band structure of the crystalline germanium, calculated using the LDA (cyan), PBE (purple), and LDA+vLB (blue) functionals. The self-consistent FP-NMTO is used to obtain electronic band structure (from $L-\Gamma-X$) and total density of states of Ge calculated. The band structures were aligned such that the valence band maximum is set at 0 eV.

the experiments. On the other hand, the vLB corrected LDA exchange within FP-NMTO formalism opens up the band-gap to 0.86 eV. Importantly, the noticeable point is the correct nature of band-gap, which is indirect along $\Gamma \rightarrow L$ matches with experiments. The valance bands remains almost same, whereas the conduction band shifted towards high energy.

The LDA and GGA, in Fig. 2, shows no sensible difference in band-structure of germanium. The spaghetti of bands originated from the Ge-4s level were seen between -13 eV and -8.7 eV (see full band-structure in supplement). The Ge-4p levels with a contribution of the Ge-4s level toward the less binding energies are found at the region closer to the Fermi energy (E_F). These bands extend from -8.7 eV up to 0 eV. The conduction band mainly results from Ge-4p with minor contributions of Ge-4s atomic orbitals toward the least excited states of Ge-4d from approximately 6.30 eV and up. Some degree of degeneracy is also observed depending on which direction of the BZ is traversed: in the $L \rightarrow \Gamma$, and $\Gamma \rightarrow X$ direction non-degenerated bands are filled with Ge-p valence electrons. The Γ directions presents 3 degenerate bands; and the X point at the edge of the BZ shows two values of energies with a twofold degeneracy.

Our first principle results show that the fundamental gap of Ge is an indirect one with the maximum of the valence band (VB_{max}) occurring at Γ and the minimum of the conduction band (CB_{min}) at the L point.^{3-9,13} The calculated indirect gap at equilibrium lattice constant is 0.86 eV (10% overestimation with respect to experiments). The calculated direct gap at the Γ point is ~ 2.0 eV. The LDA and GGA lead to the similar and direct gap of 0.19 eV and 0.33 eV, respectively. LDA+vLB estimated structural and band-gaps are in better agreement with experiments and shows improvement over beyond-DFT approaches.^{15-17,79,80}

We plot LDA, PBE and LDA+vLB calculated DOS

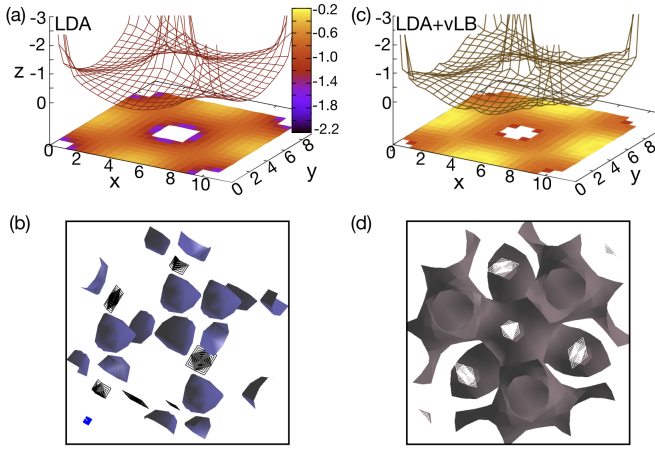


FIG. 3. (Color online) We show exchange-correlation (XC) potential for Ge, in $[100]$ -plane, calculated with FP-NMTO+ (a) LDA and (c) LDA+vLB. The z -axis represents the XC-potential surface range. The (b) LDA & (d) LDA+vLB are potential surface plots for isosurface value of -0.45 eV/C. The isosurface for Ge shows that XC-potential is less local for LDA+vLB than LDA, which helps improving the band-energies and the band-gap (see Fig. 2).

in Fig. 2 (right-panel). The DOS calculated with the FP-NMTO+vLB shows differences both in the energy positions and in the valence bandwidths with respect to LDA and PBE. We can see a weak shoulder at -0.60 eV followed by relatively broader peaks at -1.35 , -2.25 , and -2.9 eV and a sharper peak at -4.7 eV. In the conduction bands, a small shoulder can be found at 0.9 eV followed by a peak at 2.50 eV. Other peaks can be seen at 3.2 , 4.0 , and 4.8 eV. The position of DOS-points are in closer agreement with experiments.^{3-9,13,81-84} Even though Ge is known to be an *sp* material, so the correct treatment of $3d$ states is critical for accurate results. We found that major contribution of Ge- $3d$ states goes to conduction bands with smaller contribution to valence states. We consider Ge- $1s2s2p$ into the core,^{15,79,85} which leads to a better description of the band structure energies. Including Ge- $3d$ states into valence states help a better energy description and achieving fundamental (indirect) gap of Ge. Clearly, use of optimal basis set help improving fundamental behavior of Ge by improving electronic-structure. This mainly originate from the fact that the FP-NMTO uses better and improved basis representation along with vLB correction to LDA exchange.

To further elaborate, why the vLB correction in FP-NMTO produces better result, we plot XC-potential surface for LDA and LDA+vLB of Ge $[100]$ plane in Fig 3. The z -axis is representing the strength of XC-potential in the range $\{0, -3\}$. As the nature of interstitial region can not be understood for the full range of XC-potential, so, we show a truncated plot along z -axis. At atomic sites, the XC-potential forms deep wells, and falls exponentially to 0 in LDA (Fig.3(a)). However, the vLB correction makes the fall much slower than LDA (Fig.3(c)).

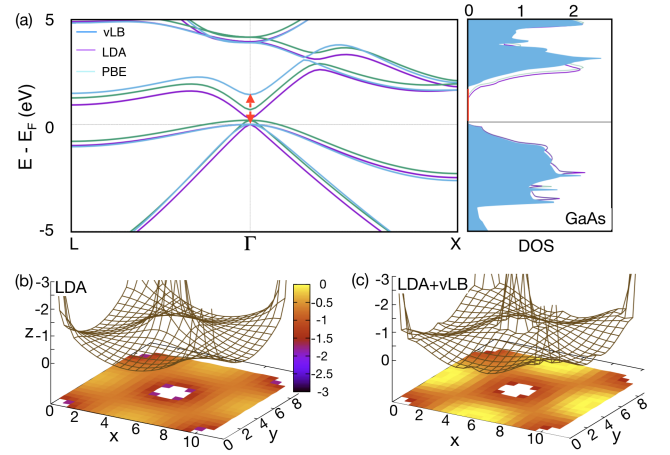


FIG. 4. (Color online) We calculate (a) electronic band-structure along $L-\Gamma-X$ (left-panel) and density of states (right-panel) of GaAs using FP-NMTO with LDA, PBE and LDA+vLB exchange-correlation potential. The FP-NMTO+vLB calculated band-gap (1.43 eV) shows good agreement with experiments (1.52 eV).⁸⁶ We also show the XC-potential surfaces corresponding to (b) LDA and (c) LDA+vLB in $[100]$ plane.

The curvature of the XC-potential surface also improves accordingly. The isosurface plots at -0.45 eV/C for LDA (Fig.3(c)) and LDA+vLB (Fig.3(d)). This shows that the XC-potential for Ge in LDA is much more localized at the atoms, but LDA+vLB has more spread over the cell.

GaAs, in ground state, crystallizes in the zinc-blende ($F\bar{4}3m$) structure,⁸⁶ where Ga and As-atoms occupy $(0, 0, 0)$ and $(1/4, 1/4, 1/4)$ sites, respectively. The ESs are placed to maintain the curvature of potential. We calculated FP-NMTO + LDA, PBE and LDA+vLB calculated band-structure and DOS in Fig. 4 (a). The band-gap calculated using FP-NMTO-LDA, PBE and LDA+vLB comes out to be 0.33 eV, 0.54 eV, and 1.43 eV, respectively. The FP-LMTO+vLB calculated band-gap of 1.43 eV shows good agreement with experimentally observed band-gap of 1.52 eV.⁸⁶ Clearly, LDA and PBE hugely underestimate the band-gap compared to LDA+vLB. Moreover, the direct (D) nature of the band-gap is also well reproduced. The band-structure and DOS in Fig. 4(a) (right-panel) does not show in constant shift in bands or density of states, which shows that vLB does not work as scissor operator. The band-structure shows larger improvement in the energy level along Γ -point than X and L, similarly, change in shape of DOS is more at the bottom of conduction band and around -2.25 eV in valence bands. In Fig. 4 (b)&(c), we plot the potential energy surface for GaAs for LDA and LDA+vLB along $[100]$, where overlapping between the potential spheres are determined self consistently. The z -axis is representing the strength of XC-potential. For clarity, we show a truncated XC-potential surface in the range $0-3$ along z -axis. We can see that at atomic sites, the XC-potential

form deep wells, and falls exponentially to 0 in LDA (Fig.4(a)) similar to Ge. The light yellow zone in Fig. 4 (c), shows smaller interstitial contribution. This is only possible if we have smaller number of interstitial electrons than LDA (darker spots). This effectively helps correcting the energy levels of conduction band.

System	a Å	NMTO			Expt.	LMTO LDA
		LDA	PBE	vLB		
Si	5.50	0.79(I)	0.845(I)	1.25(I)	1.17(I)	0.67
Ge	5.57	0.19(D)	0.33(D)	0.86(I)	0.74(I)	0.10
GaP	5.45	1.53(D)	1.68(D)	1.87(I)	2.32(I)	1.67
GaSb	6.00	0.26(D)	0.51(D)	0.94(I)	0.81(D)	0.08
GaAs	5.65	0.33(D)	0.54(D)	1.43(D)	1.52(D)	0.52
InAs	6.04	0.01(D)	0.04(D)	0.39(D)	0.43(D)	0.01
InSb	6.48	0.00(D)	0.02(D)	0.79(D)	0.23(D)	0.06
InP	5.85	0.5(D)	0.90(D)	1.18(D)	1.42(D)	0.60

TABLE I. We compare FP-NMTO calculated band-gaps for group IV and III-V materials (in eV) using LDA, PBE and LDA+vLB with LMTO-LDA. For LMTO-vLB see Ref[44]. I=indirect-band-gap; D=direct-band-gap.

The results of IV and III-V semiconductors are summarized in Table I. We show that improving the basis set (in FP-NMTO) and description of exchange-correlation functional (LDA+vLB) help reproducing better values (with exception of InSb) and correct nature of band-gap.

V. CONCLUSION

In an attempt to provide fast and efficient way to calculate band-gap of group IV and III-V semiconductors, we have developed a self consistent van Leeuwen-Baerends corrected full potential- N^{th} order muffin-tin orbital method. The band-gap of group IV and group III-V is underestimated by most semi-local exchange correlation functionals. We compare FP-NMTO+vLB calculated band-gap and electronic structure of Ge and GaAs with available experiments and theory. We show, in particular, that improved basis set and exchange-correlation potential helps in achieving better band-gaps. The proposed method can be used more effectively in calculating optical properties, localized atomic orbitals (Wannier functions), and extract real space tight-binding parameters for electronic structure study.

VI. APPENDIX

A. Structure matrix in FP-NMTO:

The definition of the structure matrix is important to form the SSWs. In the language of NMTO, the structure matrix (S^0) of LMTO is termed as Bare Structure

Matrix(B). This is found in the same way as in LMTO.

$$n_l(kr_R)Y_L(\widehat{r}_R) = \sum_{L'} j_{l'}(kr_{R'})Y_{L'}(\widehat{r}_{R'})k^{-1}B_{R'L',RL}^0(\epsilon) \quad (10)$$

$$\text{where, } k^{-1}B_{R'L',RL}^0 \equiv \sum_{l'} 4\pi(-1)^{\frac{-l+l'-l'}{2}} C_{LL'l'} \\ kn_{l'}(k|\vec{R}-\vec{R}'|)Y_{l',m'}^*(\widehat{R-R}') \quad (11)$$

$$\text{Gaunt coeff: } C_{LL'l'} = \int Y_L(\widehat{r})Y_{L'}^*(\widehat{r})Y_{l'}(\widehat{r})d\widehat{r} \quad (12)$$

If self-site terms of structure matrix is defined as $B_{R'l'm,R'l'm'}^0(\epsilon) = -\sqrt{-1}k\delta_{ll'}\delta_{mm'}$, then the one-center expansion can be written as:

$$|n^0(\epsilon, r)\rangle = |n(\epsilon, r)\rangle + k^{-1}B^0(\epsilon)|j(\epsilon, r)\rangle \quad (13)$$

The screening transformation of LMTO is made non linear in NMTO as:

$$|j^\alpha(kr)\rangle = |j(kr)\rangle - \tan \alpha_{Rlm}(\epsilon)|n(kr)\rangle \quad (14)$$

To make one center expansion similar to [eq. 13], screening transformation is found as:

$$|n^\alpha\rangle = M^\alpha|n^0\rangle = |n\rangle + k^{-1}B^\alpha|j^\alpha\rangle \quad (15)$$

Using these, the screening transformation matrix(M^α) and screened structure matrix(B^α , in LMTO it is written as S^α) is:

$$M^\alpha(\epsilon) = 1 - \frac{\tan \alpha(\epsilon)}{k}B^\alpha(\epsilon) \text{ and } B^\alpha(\epsilon) = B(\epsilon)M^\alpha(\epsilon) \\ B^\alpha(\epsilon)^{-1} = B(\epsilon)^{-1} \frac{\tan \alpha(\epsilon)}{k} \quad (16)$$

where, $k^{-1} \tan \alpha = k^{-1} \tan \alpha_{RL} \delta_{RR'} \delta_{LL'}$ is diagonal and $B^\alpha(\epsilon), B(\epsilon)$ are Hermitian.

B. Screened Spherical Waves(SSW):

The SSWs are envelop functions produced as a superposition of the Neumann's functions as:

$$|n^\alpha(\epsilon)\rangle = M^\alpha(\epsilon)|n^0(\epsilon)\rangle \quad (17)$$

The background phase shifts (α) are equal to the real phase shifts (η) in case of inactive channels.

$$|j_I^\alpha(kr)\rangle = |j_I(kr)\rangle - \tan \eta_I(\epsilon)|n(kr)\rangle \\ = -\tan \eta_I(\epsilon)|\varphi_I^0(\epsilon, r)\rangle \quad (18)$$

These screened envelop functions for inactive channels are set in a way that for inactive channels, these φ_I^0 can be substituted smoothly by the regular solutions[eq. 6] φ_I^α . This process is called "downfolding" and after this substitution the screened envelop functions become the Screened Spherical waves ψ . The MTOs are formed by the SSWs of the remaining active channels.

VII. ACKNOWLEDGEMENTS

S.D. and A.M. would like to thank Yoshiro Nohara, O. K. Andersen for permission to modify the FP-NMTO. S.D. is thankful to I Dasgupta for useful discussion. The

research at Ames Laboratory was funded from the U.S. Department of Energy (DOE), Office of Science, Basic Energy Sciences, Materials Science and Engineering Division, which is operated for the U.S. DOE by Iowa State University under contract DE-AC02-07CH11358.

-
- * prashant@ameslab.gov
- ¹ M. Nagelstraber, H. Droge, H.-P. Steinruck, F. Fischer, T. Litz, A. Waag, G. Landwehr, A. Fleszar, and W. Hanke, *Phys. Rev. B* **58**, 10394 (1998).
 - ² H. Droge, M. Nagelstrasser, J. Numberger, W. Faschinger, A. Fleszar, and H.-P. Steinrumck, *Surf. Sci.* **454**, 477 (2000).
 - ³ W.D. Grobman, D.E. Eastman, and J.L. Freeouf, *Phys. Rev. B* **12**, 4405 (1975).
 - ⁴ J.E. Ortega and F. J. Himpsel, *Phys. Rev. B* **47**, 2130 (1993).
 - ⁵ X.H. Chen, W. Ranke, and E. Schroder-Bergen, *Phys. Rev. B* **42**, 7429 (1990).
 - ⁶ M. Mohr, M. Machon, J. Maultzsch, and C. Thomsen, *Phys. Rev. B* **73**, 035217 (2006).
 - ⁷ E. Landemark, C.J. Karlsson, L.S.O. Johansson, and R. I. G. Uhrberg, *Phys. Rev. B* **49**, 16523 (1994).
 - ⁸ L. Ley, R.A. Pollak, F.R. McFeely, S.P. Kowalczyk, and D.A. Shirley, *Phys. Rev. B* **9**, 600 (1974).
 - ⁹ R.M. Feenstra, *Phys. Rev. B* **44**, 13791 (1991).
 - ¹⁰ J.A. Stroscio, R.M. Feenstra, and A.P. Fein, *Phys. Rev. Lett.* **57**, 2579 (1986).
 - ¹¹ R.M. Feenstra, J.A. Stroscio, and A.P. Fein, *Surf. Sci.* **181**, 295 (1987).
 - ¹² J.R. Chelikowsky, T.J. Wagener, J.H. Weaver, and A. Jin, *Phys. Rev. B* **40**, 9644 (1989).
 - ¹³ E. A. Kraut, R. W. Grant, J. R. Waldrop, and S. P. Kowalczyk, *Phys. Rev. B* **28**, 1965 (1983).
 - ¹⁴ E. L. Shirley, X. Zhu, and S. G. Louie, *Phys. Rev. B* **56**, 6648 (1997).
 - ¹⁵ A. Fleszar, *Phys. Rev. B* **64**, 245204 (2001).
 - ¹⁶ W. Ku, and A.G. Eguluz, *Phys. Rev. Lett.* **89**, 126401 (2002).
 - ¹⁷ P.V. Smith, M. Hermanowicz, G.A. Shah, and M.W. Radny, *Computational Materials Science* **54**, 37 (2012).
 - ¹⁸ H. Yutaka, I. Kojiro, Y. Akira, and K. Makoto, *Jpn. J. Appl. Phys.* **48**, 04C125 (2009).
 - ¹⁹ W.G. Aulbur, M. Stadele, and A. Gorling, *Phys. Rev. B* **62**, 7121 (2000).
 - ²⁰ J.P. Perdew, K. Burke, and M. Ernzerhof, *Phys. Rev. Lett.* **77**, 3865 (1996).
 - ²¹ K. Burke, J. P. Perdew, and Y. Wang, in *Electronic Density Functional Theory*, edited by M. P. Das, G. Vignale, and J. F. Dobson (Plenum, New York, 1997).
 - ²² J.P. Perdew, and A. Zunger, *Phys. Rev. B* **23**, 23, 5048 (1981).
 - ²³ J.P. Perdew, and M. Levy, *Phys. Rev. Lett.* **51**, 1884 (1983).
 - ²⁴ L.J. Sham, and M. Schlüter, *Phys. Rev. Lett.* **51**, 1888 (1983).
 - ²⁵ P. Mori-Sanchez, A.J. Cohen, and W. Yang, *Phys. Rev. Lett.* **100**, 146401 (2008).
 - ²⁶ Perry, J. K.; Tahir-Kheli, J.; Goddard, W. A. *Phys. Rev. B* **63**, 144510 (2001).
 - ²⁷ A.V. Krukau, O.A. Vydrov, A.F. Izmaylov, and G.E. Scuseria, *J. Chem. Phys.* **125**, 224106 (2006).
 - ²⁸ J.M. Crowley, J.T. Kheli, and W.A. Goddard, *J. Phys. Chem. Lett.* **7**, 1198 (2016).
 - ²⁹ S. Kümmel, and L. Kronik, *Rev. Mod. Phys.* **80**, 3 (2008).
 - ³⁰ K. Burke, and J. Chem. Phys. **136**, 150901 (2012).
 - ³¹ W. Yang, P. Mori-Sanchez, and A.J. Cohen, *AIP Conf. Proc.* **1504**, 605 (2012).
 - ³² J.P. Perdew, *MRS Bull.* **38**, 743 (2013).
 - ³³ A.D. Becke, *J. Chem. Phys.* **140** (18), 18A301 (2014).
 - ³⁴ R.O. Jones, *Rev. Mod. Phys.* **87**, 897 (2015).
 - ³⁵ H.S. Yu, S. L. Li, and D.G. Truhlar, *J. Chem. Phys.* **145**, 130901 (2016).
 - ³⁶ J. P. Perdew, A. Ruzsinszky, J. Tao, V.N. Staroverov, G.E. Scuseria, and G.I. Csonka, **123**, 062201 (2005).
 - ³⁷ M. G. Medvedev, I. S. Bushmarinov, J. Sun, J. P. Perdew, and K. A. Lyssenko, *Science* **355**, 49 (2017).
 - ³⁸ A. D. Becke, *Phys. Rev. A* **38**, 3098 (1988).
 - ³⁹ A. D. Becke, E.R. Johnson, *J. Chem. Phys.* **124**, 221101(2006).
 - ⁴⁰ N. Umezawa, *Phys. Rev. A* **74**, 032505(2006).
 - ⁴¹ R. van Leeuwen and E. J. Baerends, *Phys. Rev. A* **49**, 2421 (1994).
 - ⁴² P. Singh, M.K. Harbola, B. Sanyal and A. Mookerjee, *Phys. Rev. B* **87**, 235110 (2013).
 - ⁴³ P. Singh, M.K. Harbola, and A. Mookerjee, *Calculation of band-gaps for bulk-and nano-materials using Harbola-Sahni and van Leeuwen-Baerends Potentials*, in *Modeling, Characterization, and Production of Nanomaterials*, Ed. V.K. Tewary, and Y. Zhang (Woodhead Publishing, Massachusetts 2015), Edition 1, Vol. 1, pp. 407-418.
 - ⁴⁴ P. Singh, M.K. Harbola, M. Hemanadhan, A. Mookerjee D.D. Johnson, *Phys. Rev. B* **93**, 085204 (2016).
 - ⁴⁵ B. Sadhukhan, P. Singh, A. Nayak, S. Datta, D. D. Johnson, and A. Mookerjee, *Phys. Rev. B* **96**, 054203 (2017).
 - ⁴⁶ P. Singh, M.K. Harbola, and D.D. Johnson, *J. Phys.: Condens. Matter* **29**, 424001 (2017).
 - ⁴⁷ M. Rahaman, P. Singh, A. Mookerjee and M.K Harbola, *The band gap problem: An approach using the modified density functional theory and the Harbola-Sahni exchange potential*, in *Simulation and Characterization of the Advanced Materials Edition*, Ed. S. Kumar, (Transworld Research Network, 2010), Edition 1, Ch. 2, pp. 13-26.
 - ⁴⁸ O.K. Andersen, and T. Saha-Dasgupta, *Phys. Rev. B* **62**, R16 219 (2000).
 - ⁴⁹ H. Takeda, A. Chutinan, and S. John, *Phys. Rev. B* **74**, 195116 (2006).
 - ⁵⁰ Y. Nohara, O.K. Andersen, Interpolation across a muffin-tin interstitial using localized linear combinations of spherical waves. *Phys. Rev. B.* **94**, 101103 (2016).
 - ⁵¹ H.L. Skriver, *The LMTO Method* (Springer, New York, 1984).
 - ⁵² O.K. Andersen, *Phys. Rev. B* **12**, 3060 (1975).

- ⁵³ O.K. Andersen, O. Jepsen, and G. Krier *Lectures in Methods of Electronic Structure Calculations*, Eds.: V. Kumar, O.K. Andersen, A. Mookerjee (World Sci. Publ. Co., Singapore, 1994).
- ⁵⁴ L. Vitos *Computational Quantum Mechanics for Materials Engineers; The EMTO Method and Applications* (Springer, London, 2007).
- ⁵⁵ O. K. Andersen, C. Arcangeli, R.W. Tank, T. Saha-Dasgupta, G. Krier, O. Jepsen, I. Das-gupta *Tight-Binding Approach to Computational Materials Science*, Eds. L. Colombo, A. Gonis, P. Turchi (MRS Symposium Proceedings Series, vol 491, 1998).
- ⁵⁶ W.R.L. Lambrecht, and O.K. Andersen, Phys. Rev. B **34**, 2439 (1986).
- ⁵⁷ M.K.Y. Chan, and G. Ceder, Phys. Rev. Lett. **105**, 196403 (2010).
- ⁵⁸ D. D. Sarma, N. Shanthi, S. R. Barman, N. Hamada, H. Sawada, and K. Terakura, Phys. Rev. Lett. **75**, 1126 (1995).
- ⁵⁹ P. Hohenberg, and W. Kohn, Phys. Rev. **136**, B864 (1964).
- ⁶⁰ W. Kohn, and L.J. Sham, Phys. Rev. **140**, A1133 (1965).
- ⁶¹ U. von Barth, and L. Hedin, J. Phys. Chem. **5**, 1629 (1972).
- ⁶² G.H. Wannier, Phys. Rev. **52**, 191 (1937).
- ⁶³ J.C. Slater, Phys. Rev. **81**, 385 (1951).
- ⁶⁴ L. Hedin, and S. Lundqvist, *Solid State Phys.*, Ed. F. Seitz and D. Turnbull, (Academic Press, New York, 1969) Vol. 23, p.1.
- ⁶⁵ D.M. Ceperley and B.J. Alder, Phys. Rev. Lett. **45**, 566 (1980).
- ⁶⁶ O. Gunnarsson, and B.I. Lundqvist, Phys. Rev. B. **13**, 4274 (1976).
- ⁶⁷ R.O. Jones and O. Gunnarsson, Rev. Mod. Phys. **61**, 689 (1989).
- ⁶⁸ C.O. Almbladh and U. von Barth, Phys. Rev. B **31**, 3231(1985).
- ⁶⁹ J.P. Perdew, and Y. Wang, Phys. Rev. B **33**, 8800 (1986).
- ⁷⁰ M.K. Harbola, and V.K. Sahni, Phys. Rev. Lett. **62**, 489 (1989).
- ⁷¹ M.K. Harbola, and V.K. Sahni, Int. J. Quantum Chem. **24**, 569 (1990).
- ⁷² A. Banerjee, and M.K. Harbola, Phys. Rev. A **60**, 3599(1999).
- ⁷³ M.W. Haverkort, M. Zwierzycki, and O.K. Andersen, Phys. Rev. B **85**, 165113 (2012).
- ⁷⁴ S.H. Vosko, L. Wilk and M. Nusair, Can. J. Phys. **58** (8), 1200 (1980).
- ⁷⁵ F.D., Murnaghan, Proc. Natl. Acad. Sci. USA **30**, 244 (1944).
- ⁷⁶ I.N. Remediakis, and E. Kaxiras, Phys. Rev. B **59**, 5536 (1999).
- ⁷⁷ *Semiconductors. Physics of Group IV elements and III-V Compounds*, Ed. K. H. Hellwege and O. Madelung, *Landolt-Bornstein, New Series, Group III, Vol. 17*,(Springer, Berlin, 1982).
- ⁷⁸ J.S. Kasper, and S.M. Richards, Acta Crystallographica **17**, 752 (1964).
- ⁷⁹ M. Rohlfing, P. Krüger, and J. Pollmann, Phys. Rev. B **48**, 17791 (1993).
- ⁸⁰ M.S. Hybertsen, and S.G. Louie, Phys. Rev. B **34**, 5390 (1986).
- ⁸¹ D.E. Eastman, W.D. Grobman, J.L. Freeouf, and M. Erbudak, Phys. Rev. B **9**, 3473 (1974).
- ⁸² D. Straub, L. Ley, and F.J. Himpsel, Phys. Rev. B **33**, 2607 (1986).
- ⁸³ D.A. Muzychenko, S.V. Savinov, V.N. Mantsevich, N.S. Maslova, V.I. Panov, K. Schouteden, and C.V. Haesendonck, Phys. Rev. B **81**, 035313 (2010).
- ⁸⁴ W. B. Jackson, J. E. Northrup, J. W. Allen, and R. I. Johnson, Phys. Rev. Lett. **56**, 1187 (1986).
- ⁸⁵ E. L. Shirley, X. Zhu, and S. G. Louie, Phys. Rev. Lett. **69**, 2955 (1992).
- ⁸⁶ P. Villars, and K. Cenzual, *GaAs Crystal Structure: Datasheet* from "PAULING FILE Multinaries" in SpringerMaterials (Springer-Verlag Berlin Heidelberg, 2012)